2024 IEEE/RSJ International Conference on Intelligent Robots and Systems (IROS)
October 14-18, 2024. Abu Dhabi, UAE

Learning the Inverse Kinematics of Magnetic Continuum Robot for Teleoperated Navigation

Pingyu Xiang*, Ke Qiu*, Danying Sun, Jingyu Zhang, Qin Fang, Xiangyu Mi, Shudong Wang, Mengxiao Chen, Yue Wang, Rong Xiong, Haojian Lu†

***Abstract*— Magnetic continuum robots are subject to external magnetic fields and deformed remotely, simplifying the robot's transmission mechanism and providing it with significant potential for miniaturization and operational flexibility. However, modeling magnetic field distribution generated by permanent magnets is complex and requires time-consuming pre-calibrations. Moreover, it is highly susceptible to environments with ferromagnetic materials, posing significant challenges for the control of magnetic continuum robots. In response, we propose an approach that does not overly focus on the magnetic field distribution but instead directly learns the inverse kinematics of magnetic continuum robots end-to-end. Binding the robot's configuration to the pose of external magnets, precise control of continuum robots is facilitated. Additionally, we leverage teleoperation techniques to broaden the applicability of this method. By mounting magnets on a robotic arm and directly utilizing the target pose of the external magnet predicted by a multi-layer perceptron (MLP), we achieve the operation and navigation of magnetic continuum robots in complex environments. Experiments demonstrate that the mean control accuracy along the robot using our learning-based inverse kinematics is about half of the robot's diameter.**

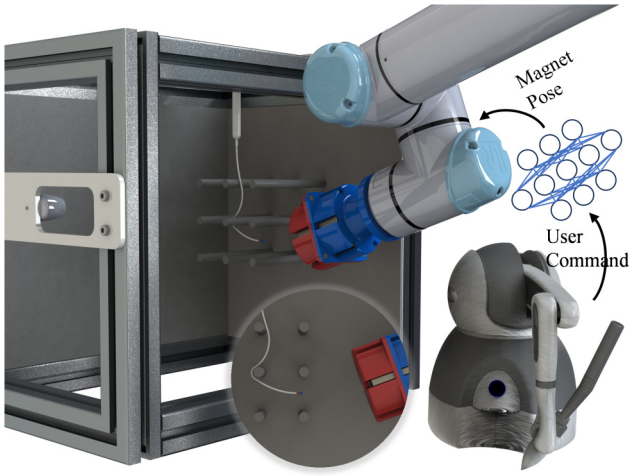

Fig. 1. Schematic representation of the application of learning-based inverse kinematics for magnetic continuum robots. The operator issues commands regarding the robot's motion and configuration through a joystick. These commands are then input into a well-trained inverse kinematics solving network, resulting in the target pose of the external magnet mounted on the robotic arm.

I. INTRODUCTION

Drawing inspiration from biological organisms such as elephant trunks, octopus tentacles, and vines [1], continuum robots have found widespread application in various unstructured environments, particularly in the medical field [2]. In contrast to traditional industrial robotic arms with discrete joints, continuum robots offer the capability for active or passive bending at any position along their body, enabling them to perform tasks in complex and dynamically changing environments.

Currently, the primary actuation methods for continuum robots include tendons [3], pneumatics [4], shape memory alloy (SMA) [5], and magnet field [6]. In contrast to the first three methods that place the transmission mechanisms directly inside the robot, magnetic actuation only requires the installation of a small permanent magnet at the robot's distal tip or doping the robot's tip with magnetized hard-magnetic particles. This allows the robot to respond to external magnetic fields and generate sufficient deformation, eliminating the transmission mechanisms within the continuum robot, such as traction cables, air bladders, or alloys. As a result, magnetic-controlled continuum robots not only avoid the nonlinear effects caused by friction in transmission devices but can also be manufactured in extremely compact sizes, enabling access to areas that bulky continuum robots cannot reach, such as the small blood vessels in the human body.

However, the advantages of magnetically actuated continuum robots come with several challenges. Firstly, the present models describing the distribution of the magnetic field are not ideal, which is adverse for obtaining the interaction force/torque between the magnetic source and robot. The commonly used multipole expansion of the point-dipole model [7], [8], which approximates the source as a magnetic dipole, is inaccurate when close to the magnet source, especially within two minimum-bounding-sphere radii [9]. Other factors such as the geometry of the magnet, material homogeneity, magnetization intensity and unpredictable fer-

*These authors contribute equally. †Corresponding author.

This work was partly supported by the National Natural Science Foundation of China (62303407), Zhejiang Provincial Natural Science Foundation of China (LD22E050007), State Key Laboratory of Electrical Insulation and Power Equipment (EIPEEIPE24212)

Pingyu Xiang, Ke Qiu, Danying Sun, Jingyu Zhang, Qin Fang, Xiangyu Mi, Yue Wang, Rong Xiong, Haojian Lu(corresponding author) are with State Key Laboratory of Industrial Control and Technology, and Institute of Cyber-Systems and Control, Zhejiang University, Hangzhou 310027, China (email: luhaojian@zju.edu.cn).

Shudong Wang is with State Key Laboratory of Electrical Insulation and Power Equipment, School of Electrical Engineering, Xian Jiaotong University.).

Mengxiao Chen is with Research Center for Humanoid Sensing, Zhejiang Lab 311100, Zhejiang Lab Nanhu Headquarters, Kechuang Avenue, Zhongtai Sub-District, Yuhang District, Hangzhou, Zhejiang Province, 311121, P.R. China).

romagnetic materials in the environment also significantly impact the magnetic field distribution around the permanent magnet. Moreover, a well-established magnetic field model is constructed either through interpolation and fitting of sampled points or by solving non-convex optimization problems with sampled points substituted into physical models [7]. Both approaches require time-consuming sampling or calibration in the preliminary stages. For now, solving for the precise magnetic field distributions around permanent magnets of arbitrary shapes, the only effective approach is numerical solutions through finite element methods, but it requires a trade-off between computational effort and speed [10]. The aforementioned issues contribute to the difficulties in the control of magnetic continuum robots.

While there are many complexities in magnetic field acquisition and robot modeling, significant research and exploration have been conducted regarding the modeling and control of continuum robots in magnetic fields. Methods proposed in [11] and [12] involve the estimation of robot configurations by minimizing the sum of magnetic potential energy and elastic potential energy. The former assumes that the magnitude and direction of the magnetic field are known and can be arbitrarily varied, while the latter employs Gauss meters to calibrate the magnetic field distribution. In [13], the authors utilize the continuation method and bifurcation analysis to obtain numerical kinematic solutions for magnetic continuum robots, which are validated through simulations and experiments in the magnetic navigation system. Using a magnetic dipole model to characterize the magnetic field generated by magnets, kinematic models for continuum robots based on the piecewise constant curvature assumption are built in [8].

With the rise of artificial neural networks, they have demonstrated impressive performance in the robotics field. In terms of kinematic modeling for continuum robots, two neural networks with ReLu activation functions addressing uncertainties and unknowns in the robot's physical model are proposed in [14], enabling cost-effective estimation of forward and inverse kinematics for concentric tube robots. In [15], the authors introduce two inverse kinematics solving networks, one for shapes represented by images and the other for discrete point representations of concentric tube robots, providing more accurate results than numerical solutions. In [16], a fully connected neural network is employed to solve the inverse kinematics of multi-section continuum robots with a simplified model of virtual rigid joints.

Therefore, to control magnetic continuum robots, neural networks can also be harnessed to achieve faster and more streamlined solutions. In this study, we introduce a learning-based approach for solving the inverse kinematics of magnetic continuum robots, eliminating the necessity for modeling the magnetic field distribution, and thus enhancing usability. We have validated and applied this method in the teleoperation control of a magnetic continuum robot navigating through obstacles, as shown in Fig. 1.

The rest of the paper is organized as follows. Section II discusses the succinct modeling of magnetic continuum robots and details the learning-based method to estimate the inverse kinematics. Section III introduces the control framework of the teleoperated magnetic continuum robot in complex environments. Section IV provides the experimental results, and finally, Section V gives the conclusion.

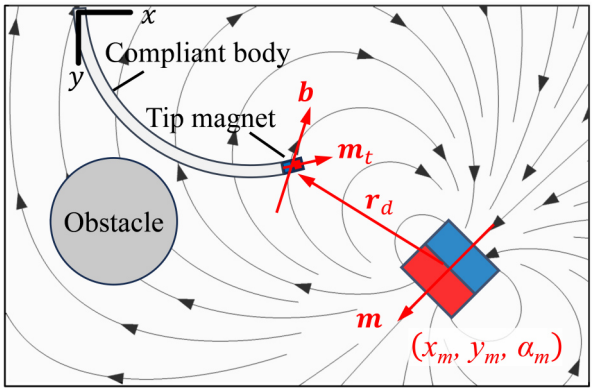

Fig. 2. The magnetic continuum robot contains a tip magnet with moment $\boldsymbol{m}_t$. The robot bends in an external field $\boldsymbol{b}$ generated by $\boldsymbol{m}$. The vector pointing from the center of the magnet to the tip is denoted by $\boldsymbol{r}_d$.

II. Learning-Based Inverse Kinematics

To specifically apply a learning-based approach to the inverse kinematics of magnetically actuated continuum robots, we initially undertake a succinct analysis of the deformations of continuum robots within magnetic fields, concluding that continuum robots constrained at the base and equipped with small permanent magnets at the tip will bend with uniform curvature. This insight is crucial for subsequently parameterizing the robot's state, which serves as the input of the neural network.

A. Modeling the Robot in Magnetic Field

Our system contains the following variables: (i) the vectors $\boldsymbol{r}, \boldsymbol{r}_t \in \mathbb{R}^2$ representing the center translation of the external magnet and the robot tip, (ii) the magnetic moments $\boldsymbol{m}, \boldsymbol{m}_t \in \mathbb{R}^2$ representing the direction of the magnet and the tip, (iii) the magnetic field $\boldsymbol{b} \in \mathbb{R}^2$ and (iv) the torque τ caused by the field exerted on the tip. We need to clarify that m, m_t, which are the magnitude of $\boldsymbol{m}, \boldsymbol{m}_t$, are constant intrinsic values of magnets.

According to [17], we have the following relationship between the curvature κ and the torque τ exerted on the tip,

$$EI\kappa = \tau, \tag{1}$$

where I is the cross-sectional moment of inertia, E the Young's modulus and the product EI the bending stiffness. Since the curvature does not vary along the length of the robot, we can consider the robot's shape under the influence of the magnetic field to be an arc.

The magnetic field is regarded as being generated at $\boldsymbol{r}$ by a magnetic moment $\boldsymbol{m}$ with the field $\boldsymbol{b}$, as shown in Fig. 2,

and we have the following definition,

$$\boldsymbol{r}_d = \boldsymbol{r}_t - \boldsymbol{r}, \tag{2}$$

where $\boldsymbol{r}_t$ represents the robot tip translation, $\boldsymbol{r} = \begin{pmatrix} x_m & y_m \end{pmatrix}^{\mathrm{T}}$ represents the magnet center translation and α_m the orientation. If the curvature κ and the length of the robot L are given, we know the position and orientation of the tip magnet, i.e.,

$$\boldsymbol{r}_t = \frac{1}{\kappa} \begin{pmatrix} 1 + \cos \kappa L & \sin \kappa L \end{pmatrix}^{\mathrm{T}} \tag{3}$$

and

$$\hat{\boldsymbol{m}}_t = \begin{pmatrix} \sin \kappa L & \cos \kappa L \end{pmatrix}^{\mathrm{T}}. \tag{4}$$

Note that $\hat{\boldsymbol{m}}_t$ represents the unit vector of $\boldsymbol{m}_t$, that is $\boldsymbol{m}_t = m_t \hat{\boldsymbol{m}}_t$. We also adopt this notation for the remaining variables in the rest of this paper.

According to [7], The magnetic field vector $\boldsymbol{b}$ at point $\boldsymbol{r}_t$ is mainly influenced by the relative position vector $\boldsymbol{r}_d$ and the magnetic moment vector $\boldsymbol{m}$, representing as

$$\boldsymbol{b} = B\left(\boldsymbol{r}_d, \boldsymbol{m}\right), \tag{5}$$

where B is often regarded as either the magnetic dipole model or the elliptic integral model in many other research.

When the robot is placed at the field $\boldsymbol{b}$, since a small permanent magnet $\boldsymbol{m}_t$ is mounted at the tip of the continuum robot, the tip is compelled to translate and rotate, attempting to align with that field. However, the variation of the field is always small enough so that the force pulling the tip along the field gradient is negligible [11]. As a result, only the external torque τ is considered, so we have

$$\tau = \boldsymbol{m}_t \times \boldsymbol{b} = m_t b \det\begin{pmatrix} \hat{\boldsymbol{m}}_t & \hat{\boldsymbol{b}} \end{pmatrix}. \tag{6}$$

Finally, equations (1)-(6) constitute the succinct system model. Through this modeling process, we can theoretically calculate the specific behavior of the robot under the magnetic field. We can also calculate the posture of the external magnet to apply a proper magnetic field, steering the robot to navigate in complex environments.

However, existing magnetic models B are not sufficiently accurate across all spatial domains, and the distribution of the magnetic field $\boldsymbol{b}$ can be easily influenced by ferromagnetic materials, let alone some extra calibrations are necessary to obtain the exact value of the magnetic moment $\boldsymbol{m}$ and $\boldsymbol{m}_t$, which all make the inverse kinematics problem rocky to solve analytically.

In this paper, we pay special attention to inverse kinematics, which is crucial for path planning, object manipulation, and control. With a simplified model presented, we propose a data-driven method to obtain a proper placement of the external magnet with known robot length and desired curvature.

B. Learning-Based Method for Inverse Kinematics

Considering the difficulties in magnetic field acquisition and the complexity of the calibration process mentioned in Section I, we employ feedforward neural networks to address these issues.

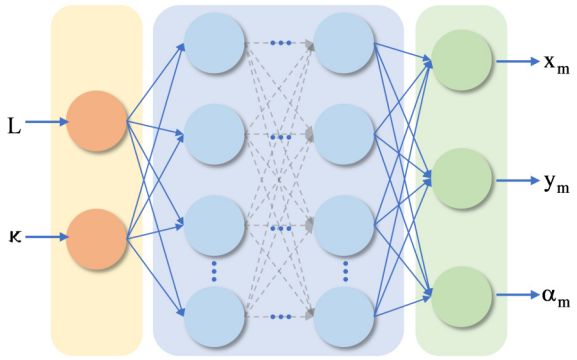

Fig. 3. The schematic diagram of a Multi-layer Perceptron (MLP), from left to right, consists of the input layer, hidden layers, and output layer. The arrows connecting the nodes represent learnable weights and the direction of signal propagation.

The motivation of this learning-based method includes but is not limited to the following. Firstly, Neural networks naturally incorporate the strong nonlinearity and uncertainty of magnetic field distribution into the intermediate process, which enables direct end-to-end learning of the relationship between robot configurations and magnet positions and orientations, avoiding the need for complex and time-consuming magnetic field modeling. Additionally, a well-trained neural network outputs the most reasonable and realistic position and orientation of the magnet based on the data distribution in the training dataset, avoiding the multi-solution dilemma mentioned in [18].

The MLP we use, as shown in Fig. 3, is a type of artificial neural network (ANN) commonly employed for various machine learning and deep learning tasks. It serves as an excellent function approximator. The MLP consists of three main components: an input layer, several hidden layers, and an output layer, with each layer containing multiple neurons (as indicated by the coloured circles in Fig. 3). Utilizing techniques like backpropagation and gradient descent, the network learns the optimal mapping between input and output based on the error between the output and the ground truth.

For solving the inverse kinematics problem of magnetic continuum robots, the network takes the current segment's length L, and the desired robot curvature κ as input. The output consists of the translation x_m, y_m, and the orientation α_m of the external magnet, as depicted in Fig. 3.

III. Control of Teleoperated Magnetic Continuum Robot

The teleoperated control application scenario for our proposed learning-based inverse kinematics of magnetic continuum robots is illustrated in Fig. 4. In this scenario, an operator manipulates a joystick, employing a method similar to the teleoperation mapping discussed in [19], which intuitively translates the operator's actions into parameters within the robot's configuration space. Once the command of the desired configuration (curvature κ and length L) is achieved, it is input into the well-trained MLP, which

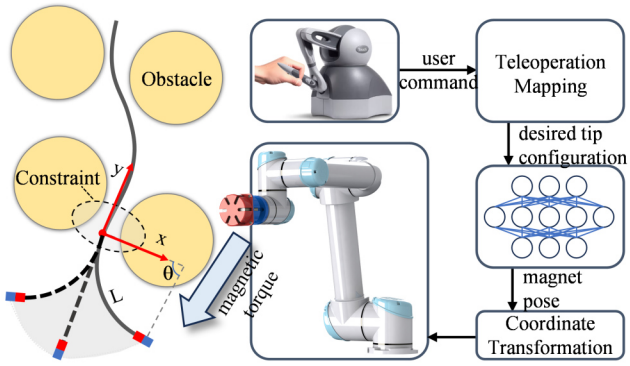

Fig. 4. The controlled scenario of magnetic continuum robot in a multi-contact environment and the schematic diagram of teleoperation control.

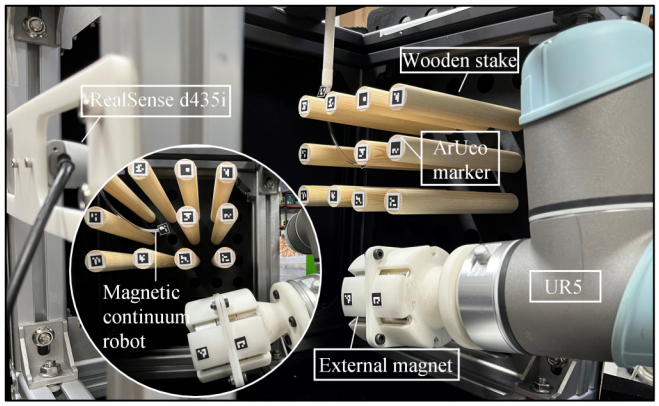

Fig. 5. Experimental setup of the magnetic robot system for data collection and experimental validation.

accordingly outputs the magnet translation and orientation for further control.

It's worth noting that in our previous analyses, we assumed that only the base of the robot was constrained. However, in situations where the robot navigates through complex and narrow environments with multiple points of contact, aside from the free part, the rest of the robot is constrained by obstacles. In such cases, the nearest contact point to the robot's head is considered the new base of the robot. By defining a local coordinate system with this constraint point as the origin, the robot's length L and bending angle θ can be redefined as shown on the left side of Fig. 4, allowing us to directly utilize the conclusions from a single robot segment and the pre-trained inverse kinematics network.

Therefore, the network outputs the magnet's position and orientation in the local coordinate system (labelled as $x-y$ in Fig. 4) and requires a coordinate transformation to the world coordinate system so that the magnet can apply a proper magnetic torque on the robot's tip.

IV. EXPERIMENT AND RESULT

In this section, a series of experiments are conducted to validate the proposed method. To begin with, we conduct basic robot characterization experiments to explore the robot's workspace. We then collect relevant data to train neural networks and performed inverse kinematics solving tests on the test dataset as well as on the physical robot. Finally, we demonstrate the teleoperated control of the magnetic continuum robot as it navigates through wooden stakes via various paths.

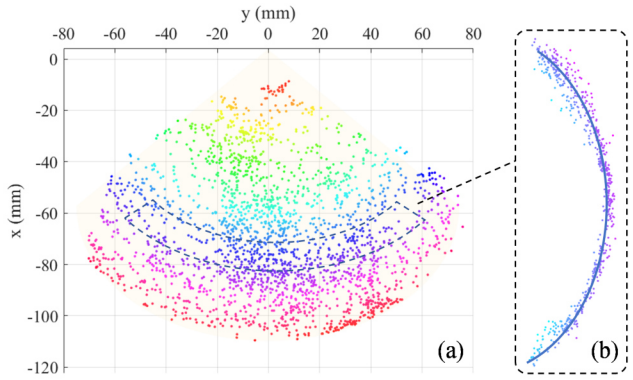

Fig. 6. Point cloud of workspace. (a) The workspace of the magnetic continuum robot as length ranges from 20 mm to 110 mm. (b) The trajectory when the robot is 80 mm in length.

A. Robot Characteristics and Representations

The magnetic teleoperated continuum robot system and experimental setup we employed are depicted in Fig. 5. This system primarily consists of a magnetic continuum robot, a permanent magnet mounted on the UR5 robotic arm, a RealSense d435i camera for providing a comprehensive environmental view, evenly spaced wooden stakes as obstacles, and ArUco markers for localization [20]. All devices are housed within an aluminium frame to minimize the impact of ferromagnetic materials on the magnetic field distribution.

Specifically, our magnetic continuum robot is constructed using polyvinyl chloride (PVC) tubes with an outer diameter of 3 mm and an inner diameter of 2 mm. The tube tip is embedded with small-size N52 cylindrical magnets, and we can vary the robot's effective length through an advancer. ArUco markers are utilized to estimate the positions and orientations of external magnets, the robot's head, and the positions of various obstacles relative to the camera in cluttered scenes.

Fig. 6 illustrates the workspace of the magnetic continuum robot. By controlling the magnitude and direction of the external magnetic field, the robot can bend in different directions. As we extend its effective length from 20 mm to 110 mm, ultimately, an approximately 102° sector-shaped workspace is acquired and shown in Fig. 6(a). The trajectory when the robot's length is 80 mm is demonstrated in Fig. 6(b). The reason for the workspace presenting a sector shape lies in the fact that, under the same bending moment, the maximum deflection of a beam increases with its length.

Fig. 7 (a) showcases the bending states of the magnetic continuum robot under external magnetic fields with the robot's length of 100 mm. We select five representative postures, and on the robot's backbone, 15 evenly distributed reference points are selected. We applied the single-section

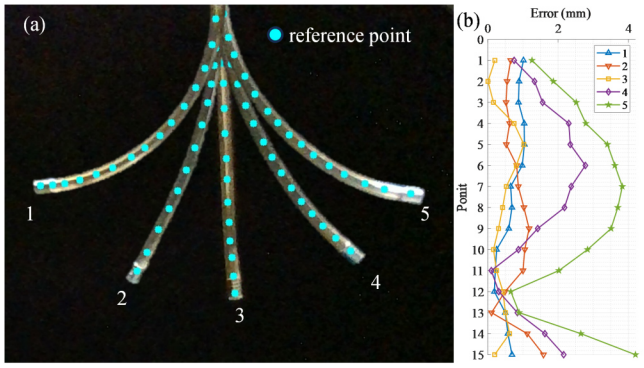

Fig. 7. The feasibility of constant curvature assumption. (a) Five representative postures of the continuum robot with 15 reference points attached to the body. (b) The error plot of the circular arc fitting.

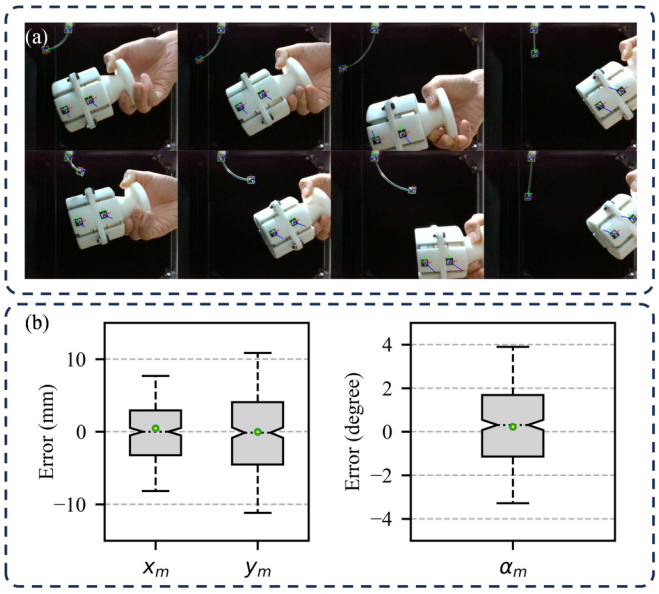

Fig. 8. Data collection and performance of MLP. (a) Collecting data of different lengths and curvature. (b) The performance of the trained neural network on test set.

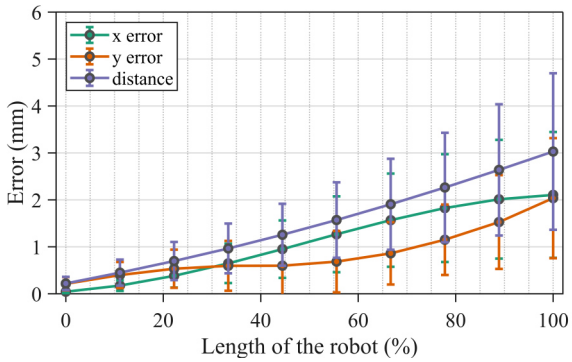

Fig. 9. Error plot of the learning-based inverse kinematics along the actual robot body.

circular arc mentioned in Section II to fit these reference points separately. The fitting errors for each point on each posture group are displayed in Fig. 7(b). The average fitting error for 75 points is 1.21 mm, 1.21% of the robot's length. The largest fitting error is 4.19 mm. Hence, it is evident that using circular arcs to fit the magnetic continuum robot is entirely reasonable.

B. Data Acquisition and Performance of the Neural Network

The training of the MLP is a supervised process, thus requiring the collection of a sufficient amount of training data. Fig. 8(a) illustrates the data collection process, where ArUco markers are attached to both ends of the robot and the external magnet. This allows us to simultaneously collect data of the robot's length (L), curvature (κ), and the position (x_m, y_m) and orientation (α_m) of the external magnet.

Approximately 3000 valid data samples were acquired and randomly split into a training set and a test set in a 7:3 ratio. To expedite convergence, the input data was min-max normalized, and the network was trained using the Adam optimizer in the PyTorch framework with a batch size of 64. The mean squared error (MSE) loss function was employed. The training was halted when the training set loss ceased to decrease, and there was no rebound in the test set loss to prevent overfitting.

The performance of the trained neural network on the test set is depicted in Fig. 8(b). For each combination of robot length (L) and curvature (κ) in the test set, the mean absolute errors for magnet position and orientation are 4.43 mm, 5.02 mm, and 1.58°, respectively, which is acceptable compared with the geometric dimension of the magnet (height 60 mm, diameter 68 mm).

We further conducted control experiments on the physic robot system. We set the desired robot's length (L_t) using the advancer and target curvature (κ_t) arbitrarily, by which we define the ideal arc of the robot. Then, inputting these values into the trained neural network could obtain the expected magnet translation (x_m, y_m) and orientation (α_m). We then control the robotic arm to the corresponding pose and fit the bent robot with a circular arc (the actual arc). After conducting several experiments and comparing these two kinds of arcs (actual and ideal arcs), the average control errors along the actual robot body are analyzed, as shown in Fig. 9. We define the error by calculating the Euclidean distance between the equally distributed points along the actual and ideal arc. This method achieved an average error of 1.09 mm, 0.86 mm, and 1.50 mm in the x, y, and distance, respectively. The robot's end effector is the part with the highest error, with an error of 2.10 mm, 2.03 mm, and 3.02 mm, respectively. The experiments demonstrate that compared with the robot's diameter (3 mm), the learning-based inverse kinematics control errors are within a reasonable range and can accurately control the robot's configuration and end-effector to the desired placement.

C. Dexterity of Teleoperated Navigation

In the final phase of our experiments, we teleoperate the robot navigating through obstacles, following the same basic setup as depicted in Fig. 5. The operator, located

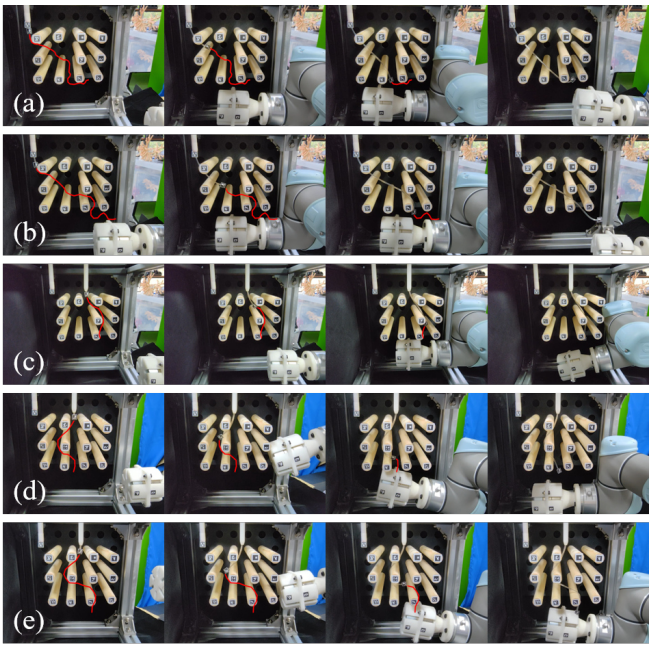

Fig. 10. Experiments involving teleoperated magnetic continuum robot navigating through obstacle wooden stakes, where (a) to (e) represent five different sets of the experiments, and the trajectory of the robot's end-effector is indicated by a red curve.

remotely, control the robot using a joystick, extending the robot downward while adjusting its direction. Simultaneously, the robotic arm responds to the operator's commands, moving the magnet to the inferred position obtained through the neural network for real-time obstacle avoidance and navigation.

Five sets of navigation experiments are illustrated in Fig. 10(a)-(e). In each experiment, the robot successfully navigates through different obstacles and reaches distinct target positions with great dexterity. The end-effector trajectories of the robot in these five experiments are depicted by red curves. These experiments demonstrated that our proposed inverse kinematics solution algorithm can be effectively applied for real-time navigation control of magnetic robots.

V. CONCLUSION

In this paper, we have proposed learning-based inverse kinematics of magnetic continuum robots, which tackle the challenges posed by the inherent uncertainties associated with magnetic field distributions. We begin by conducting a simplified modeling of the magnetic continuum robot and elucidate the complexities related to the calibration and characterization of the magnetic field distribution.

Our proposed method is validated through a combination of extensive dataset tests and physical robot experiments. We are confident that the performance of this approach will witness significant enhancements as we continue to fine-tune hyperparameters and expand our dataset, thereby pushing the boundaries of its capabilities.

REFERENCES

[1] M. Wooten, C. Frazelle, I. D. Walker, A. Kapadia, and J. H. Lee, "Exploration and inspection with vine-inspired continuum robots," in *2018 IEEE International conference on robotics and automation (ICRA)*. IEEE, 2018, pp. 5526–5533.

[2] J. Burgner-Kahrs, D. C. Rucker, and H. Choset, "Continuum robots for medical applications: A survey," *IEEE Transactions on Robotics*, vol. 31, no. 6, pp. 1261–1280, 2015.

[3] T.-D. Nguyen and J. Burgner-Kahrs, "A tendon-driven continuum robot with extensible sections," in *2015 IEEE/RSJ International Conference on Intelligent Robots and Systems (IROS)*. IEEE, 2015, pp. 2130–2135.

[4] J. D. Greer, T. K. Morimoto, A. M. Okamura, and E. W. Hawkes, "Series pneumatic artificial muscles (spams) and application to a soft continuum robot," in *2017 IEEE International Conference on Robotics and Automation (ICRA)*. IEEE, 2017, pp. 5503–5510.

[5] Y. Goergen, G. Rizzello, S. Seelecke, and P. Motzki, "Modular design of an sma driven continuum robot," in *Smart Materials, Adaptive Structures and Intelligent Systems*, vol. 84027. American Society of Mechanical Engineers, 2020, p. V001T04A007.

[6] Y. Kim, G. A. Parada, S. Liu, and X. Zhao, "Ferromagnetic soft continuum robots," *Science Robotics*, vol. 4, no. 33, p. eaax7329, 2019.

[7] J. J. Abbott, E. Diller, and A. J. Petruska, "Magnetic methods in robotics," *Annual Review of Control, Robotics, and Autonomous Systems*, vol. 3, pp. 57–90, 2020.

[8] G. Pittiglio, A. L. Orekhov, T. da Veiga, S. Calò, J. H. Chandler, N. Simaan, and P. Valdastri, "Closed loop static control of multi-magnet soft continuum robots," *IEEE Robotics and Automation Letters*, 2023.

[9] A. J. Petruska and J. J. Abbott, "Optimal permanent-magnet geometries for dipole field approximation," *IEEE transactions on magnetics*, vol. 49, no. 2, pp. 811–819, 2012.

[10] A. Caciagli, R. J. Baars, A. P. Philipse, and B. W. Kuipers, "Exact expression for the magnetic field of a finite cylinder with arbitrary uniform magnetization," *Journal of Magnetism and Magnetic Materials*, vol. 456, pp. 423–432, 2018.

[11] I. Tunay, "Modeling magnetic catheters in external fields," in *The 26th Annual International Conference of the IEEE Engineering in Medicine and Biology Society*, vol. 1, 2004, pp. 2006–2009.

[12] D. Lin, N. Jiao, Z. Wang, and L. Liu, "A magnetic continuum robot with multi-mode control using opposite-magnetized magnets," *IEEE Robotics and Automation Letters*, vol. 6, no. 2, pp. 2485–2492, 2021.

[13] Q. Peyron, Q. Boehler, K. Rabenorosoa, B. J. Nelson, P. Renaud, and N. Andreff, "Kinematic analysis of magnetic continuum robots using continuation method and bifurcation analysis," *IEEE Robotics and Automation Letters*, vol. 3, no. 4, pp. 3646–3653, 2018.

[14] R. Grassmann, V. Modes, and J. Burgner-Kahrs, "Learning the forward and inverse kinematics of a 6-dof concentric tube continuum robot in se (3)," in *2018 IEEE/RSJ International Conference on Intelligent Robots and Systems (IROS)*. IEEE, 2018, pp. 5125–5132.

[15] N. Liang, R. M. Grassmann, S. Lilge, and J. Burgner-Kahrs, "Learning-based inverse kinematics from shape as input for concentric tube continuum robots," in *2021 IEEE International Conference on Robotics and Automation (ICRA)*. IEEE, 2021, pp. 1387–1393.

[16] J. Lai, K. Huang, and H. K. Chu, "A learning-based inverse kinematics solver for a multi-segment continuum robot in robot-independent mapping," in *2019 IEEE International Conference on Robotics and Biomimetics (ROBIO)*. IEEE, 2019, pp. 576–582.

[17] I. A. Gravagne, C. D. Rahn, and I. D. Walker, "Large deflection dynamics and control for planar continuum robots," *IEEE/ASME transactions on mechatronics*, vol. 8, no. 2, pp. 299–307, 2003.

[18] D. Lin, N. Li, N. Jiao, Z. Wang, and L. Liu, "Kinematic analysis of multi-section opposite magnetic catheter robots with solution multiplicity," *IEEE Transactions on Automation Science and Engineering*, pp. 1–12, 2022.

[19] M. Csencsits, B. A. Jones, W. McMahan, V. Iyengar, and I. D. Walker, "User interfaces for continuum robot arms," in *2005 IEEE/RSJ International Conference on Intelligent Robots and Systems*. IEEE, 2005, pp. 3123–3130.

[20] M. Kalaitzakis, B. Cain, S. Carroll, A. Ambrosi, C. Whitehead, and N. Vitzilaios, "Fiducial markers for pose estimation: Overview, applications and experimental comparison of the artag, apriltag, aruco and stag markers," *Journal of Intelligent & Robotic Systems*, vol. 101, pp. 1–26, 2021.